Supporting Information

Adsorption of 2,4-D dichlorophenoxyacetic acid in an aqueous media on nanoscale MIL-53(Al) type materials

Vera I. Isaeva[a,b]*, Marina D. Vedenyapina[a], Stanislav A. Kulaishin[a], Anna A. Lobova[c], Vladimir V. Chernyshev[c], Gennady I. Kapustin[a], Olga P. Tkachenko[a], Vadim V. Vergun[a], Danil A. Arkhipov[a], Vera D. Nissenbaum[a], and Leonid M. Kustov[a,b,c]*

a N.D. Zelinsky Institute of Organic Chemistry, Russian Academy of Sciences, Leninsky prospect 47, Moscow 119991, Russia
b National University of Science and Technology MISiS, Leninsky prosp. 4, Moscow 119991, Russia
c Department of Chemistry, M.V. Lomonosov Moscow State University, 1-3 Leninskie Gory, Moscow 119991, Russian Federation

*Corresponding author. Tel./Fax: +749913729835.
E-mail address: sharf@ioc.ac.ru

Content

I. Efficiency of the activation (pore deliberation) of the synthesized **MixLR** materials with mixed bdc and abdc linkers.

II. TEM study of the dispersion of **MixLR** materials

III. Structural examinations of the synthesized MIL-53(Al) type materials.

IV. New crystal structure determination from two-phase synchrotron powder pattern.

V. Study of the thermal stability of MIL-53(Al) type materials

VI. DRIFTS investigations of MIL-53(Al) type materials

VII. Study of the pH effect on the 2,4-D adsorption o **MixL2R** material

I. *Efficiency of the activation (pore deliberation) of the synthesized **MixLR** materials with mixed bdc and abdc linkers*

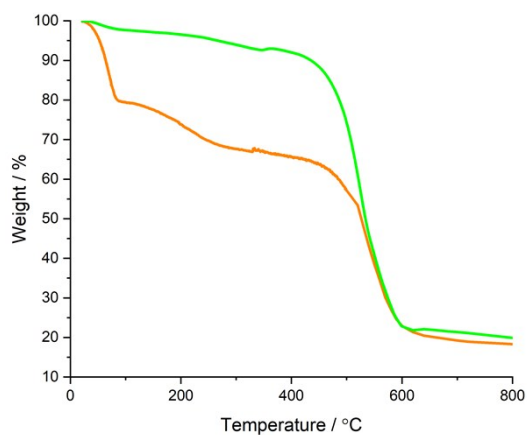**Figure S1**. TG curves for **MixL3R** (green) and **MixL3** (orange) samples.

a)   b) .
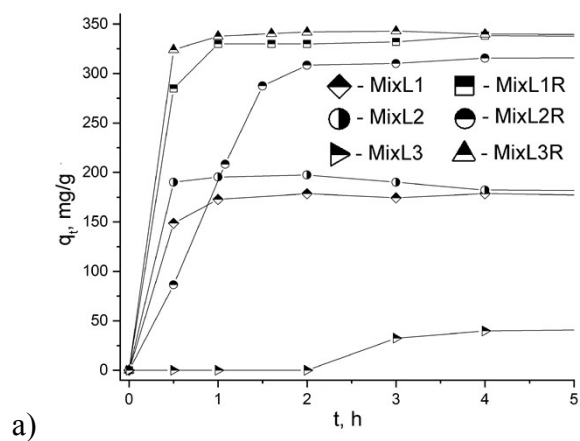
Figure S2. Comparison of 2,4-D adsorption curves for **MixL** and **MixLR** materials for 5 h (a) and 225 h (b).

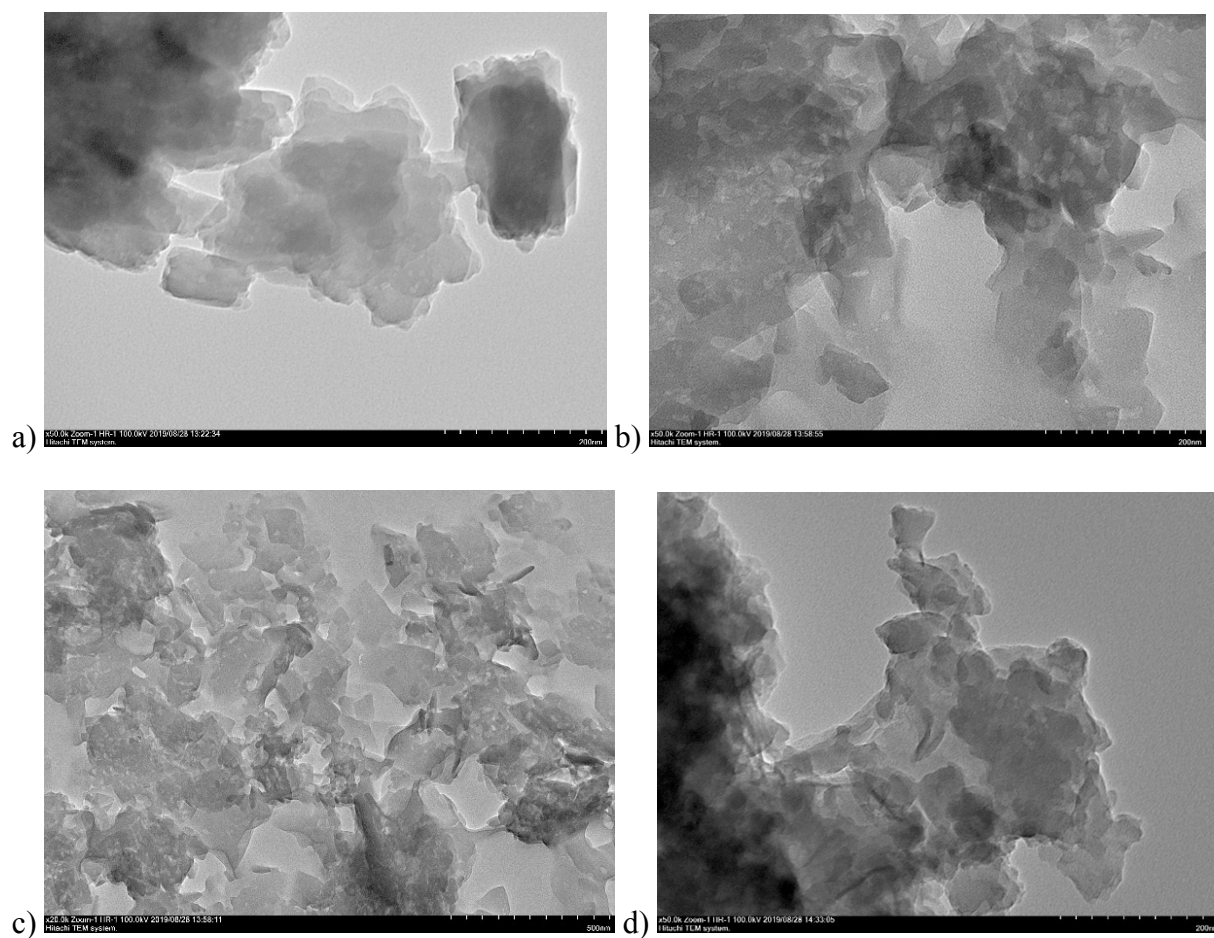**II.** *TEM study of the dispersion of **MixLR** materials*

Figure S3. TEM images for MixLR1(a), MixLR2 (b, c), and MixLR3 (d) materials.

III. *Structural examinations of the synthesized MIL-53(Al) type materials*
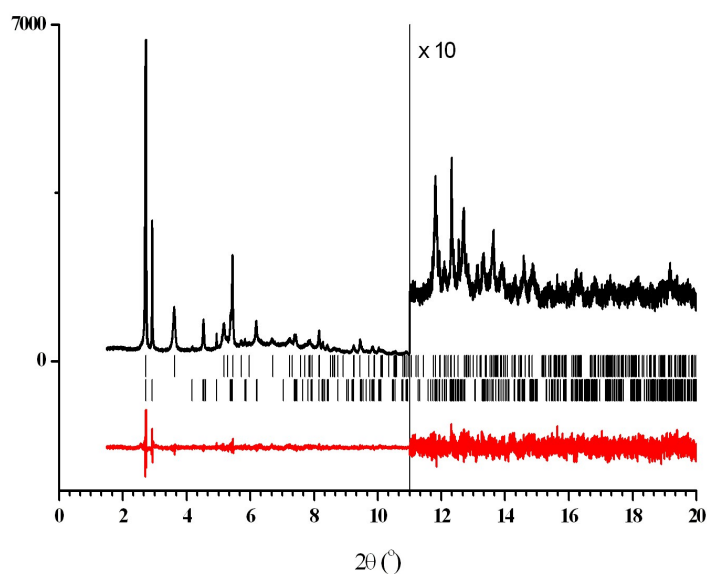

Figure S4. The final Rietveld plot for the synchrotron pattern of the NH_2-MIL-53(Al) sample showing the experimental (black) and difference (red) curves. The vertical bars denote calculated positions of the peaks for two phases – monoclinic *Cc* (1st raw) and monoclinic *I2/m* (2nd raw).
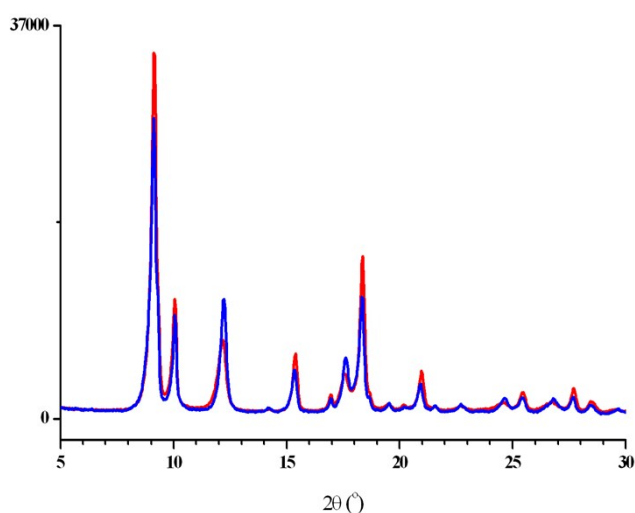

Figure S5. Comparison of laboratory powder patterns of NH_2-MIL-53(Al) (red) and NH_2-MIL-53(Al)$_{SHF}$ (blue) – before and after SHF treatment, respectively. Small changes in the intensities of separate peaks corresponding to one phase solely, for instance, at $2\theta = 10.05°$ (*ht* phase, monoclinic *I2/m*, *hkl = 020*) and 12.25° (*lt* phase, monoclinic *Cc*, *hkl = 110*), demonstrate a weak redistribution of the phase ratio in favor of the *lt* phase.
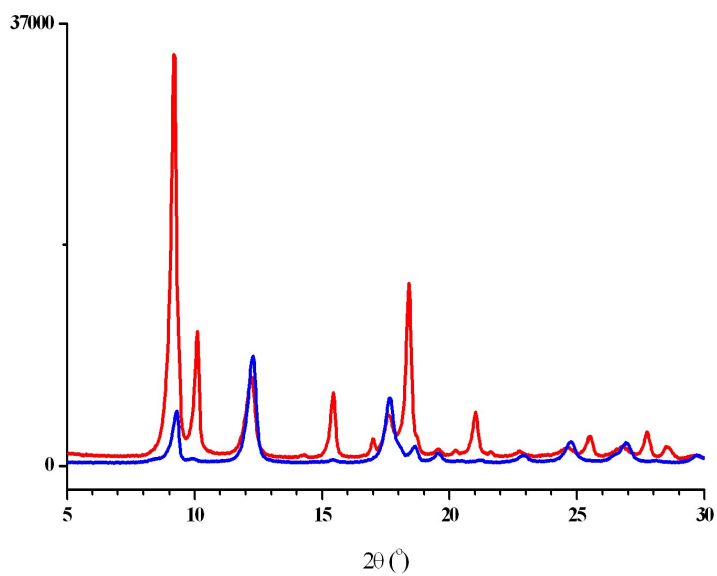
Figure S6. Laboratory powder patterns of NH_2-MIL-53(Al) before (red) and after (blue) 2,4-D adsorption.
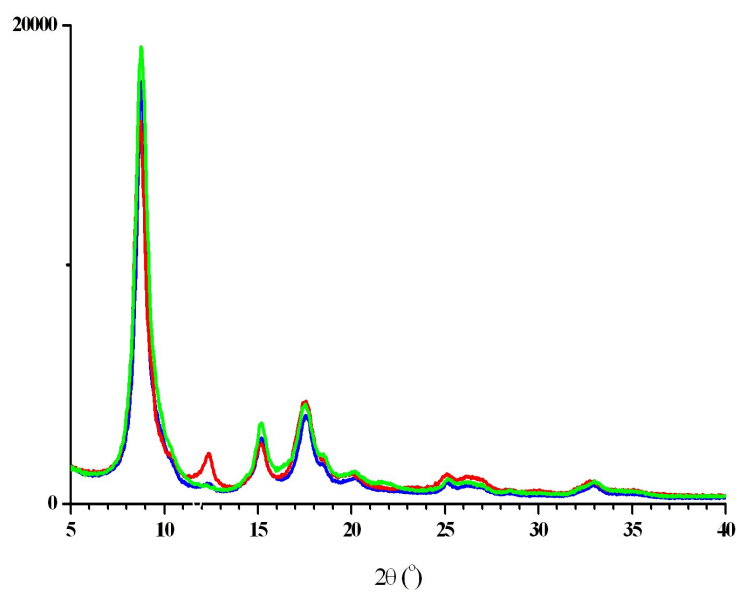

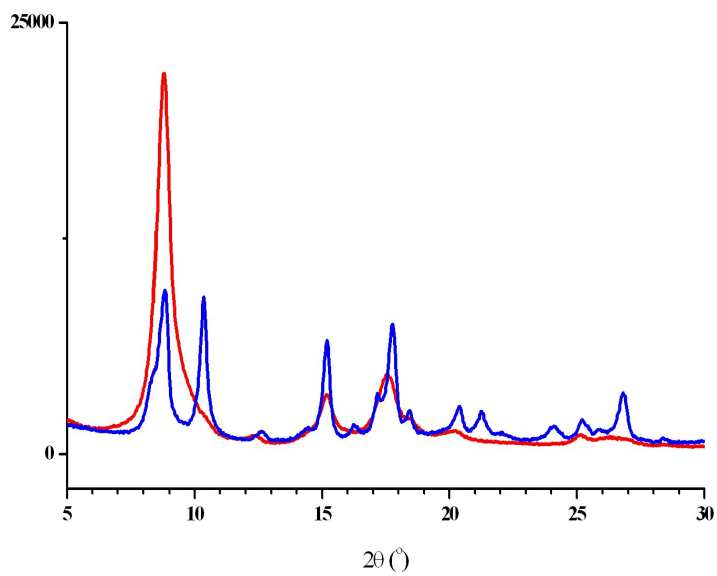**Figure S7**. Laboratory powder patterns of **MixL1R** (blue), **MixL2R** (red) and **MixL3R** (green).

Figure S8. Laboratory powder patterns of **MixL1R** before (red) and after (blue) 2,4-D adsorption.

IV. *New crystal structure determination from the two-phase synchrotron powder pattern*.

The low-temperature ($T = 200$ K) X-ray measurement of NH_2-MIL-53(Al) has shown that it contains more than one crystalline phase. One phase was unequivocally identified as monoclinic *Cc* isostructural to NH$_2$-MIL-53(Al)*lt* (CSD refcodes *NAXLEF* [1]). Therefore, all separate peaks associated with this crystal structure were excluded from further consideration at the stage of indexing. The positions (*d*-spacings) of the rest 16 low-angle peaks (see Table **S1**) were used in attempts to index them in one unit cell.

Table S1. List of *d*-spacings used in indexing of new monoclinic structure (*I2/m*).

	d, Å	I, %
1	9.4976	100
2	8.8695	39
3	6.2100	1
4	5.7090	10
5	5.2361	3
6	4.8072	7
7	4.7512	28
8	4.4349	1
9	4.1814	8
10	4.0759	1
11	3.8716	2
12	3.5008	2
13	3.4804	3
14	3.1688	5
15	3.1272	2
16	3.0729	2

Three indexing programs - *TREOR90* [2], *DICVOL06* [3] and *AUTOX* [4, 5] – were used, and all of them resulted in two concurrent I-centered cells – orthorhombic (*a, b, c* = 6.64, 17.71, 11.28 Å) and monoclinic (*a, b, c* = 6.64, 17.74, 11.25 Å, β = 90.36°). However, monoclinic parameters produced a much better M_{16} indicator (~30) as compared with orthorhombic ones (M_{16}~12). Further, the Pawley fit [6] for each new I-centered cell with the simultaneous Rietveld refinement (with fixed atomic coordinates taken from the *NAXLEF* structure) for the known NH$_2$-MIL-53(Al)*lt* structure led to results significantly differing in the value of χ^2 (=1.83 with monoclinic parameters, and 5.44 with orthorhombic ones even in the space group *Imm2*) and in the number of indexed peaks. The monoclinic cell was preferable for all indicators. Therefore, the monoclinic unit cell was chosen for the crystal structure determination of the second crystalline phase of the NH_2-MIL-53(Al) sample.

Three possible monoclinic space groups – *I2*, *Im* and *I2/m* – were tested in attempts to solve the new crystal structure. The crystal structure was solved in the space group *I2/m* with the use of a simulated annealing technique [7] based on the set of 120 low-angle X_{obs} values [8] extracted from the two-phase synchrotron powder pattern after a Pawley fit following the methodology used by us earlier in the crystal structure determinations from multi-phase powder patterns [9-11]. To take properly into account the presence of solvent molecules (*dmfa*, H_2O) disordered in the pores, their rigid models with the occupancies fixed to 0.5 were also used in simulated annealing runs.

The final two-phase Rietveld refinement was performed with the program MRIA [12] following the procedure described by us previously [9-11]. In the refinement, anisotropic line broadening was taken into account for each crystalline phase (Popa, 1998). All non-H atoms were refined isotropically, additional constraints for U_{iso} were applied to limit the number of variables. Namely, only two common U_{iso} parameters were refined – one parameter for all non-H atoms of the framework and another one for non-H atoms of disordered solvent molecules. Crystal data, data collection and structure refinement details are summarized in Table **S2** and the diffraction profiles after the final bond-restrained Rietveld refinement are shown in Fig. S4. This crystal structure has been deposited in the Camdridge Structural Database under No. 1934522.

In Fig. S9, prepared with *Mercury* [14], one can see the 3D framework (without solvent molecules) of this new monoclinic structure, which can be considered as some distortion of the classic orthorhombic framework caused by the incorporation of *dmfa* and H_2O molecules into pores (Fig. S10).

Table S2. Crystallographic data for new monoclinic *I2/m* phase (two-phase refinement).

	Phase *I2/m*
Empirical formula	$[C_8H_{28}AlNO_5, C_3H_7NO, H_2O]$
Formula weight	313.22
Crystal system	monoclinic
Space group	*I2/m*
a, Å	6.6264(9)
b, Å	17.7350(18)
c, Å	11.2621(14)
β, deg	90.311(9)
V, Å^3	1323.5(3)
Z	4
Diffractometer	ID22, ESRF
Radiation	synchrotron
Wavelength, Å	0.450851(3)
ρ_{calc}, g/cm^3	1.572
μ, mm^{-1}	0.108
$2\theta_{min} - 2\theta_{max}$, increment, deg	1.500 – 20.000, 0.002
Number of parameters/restraints	123/125
$R_p/R_{wp}/R_{exp}$	0.0500/0.0625/0.0437
goodness-of-fit	1.395

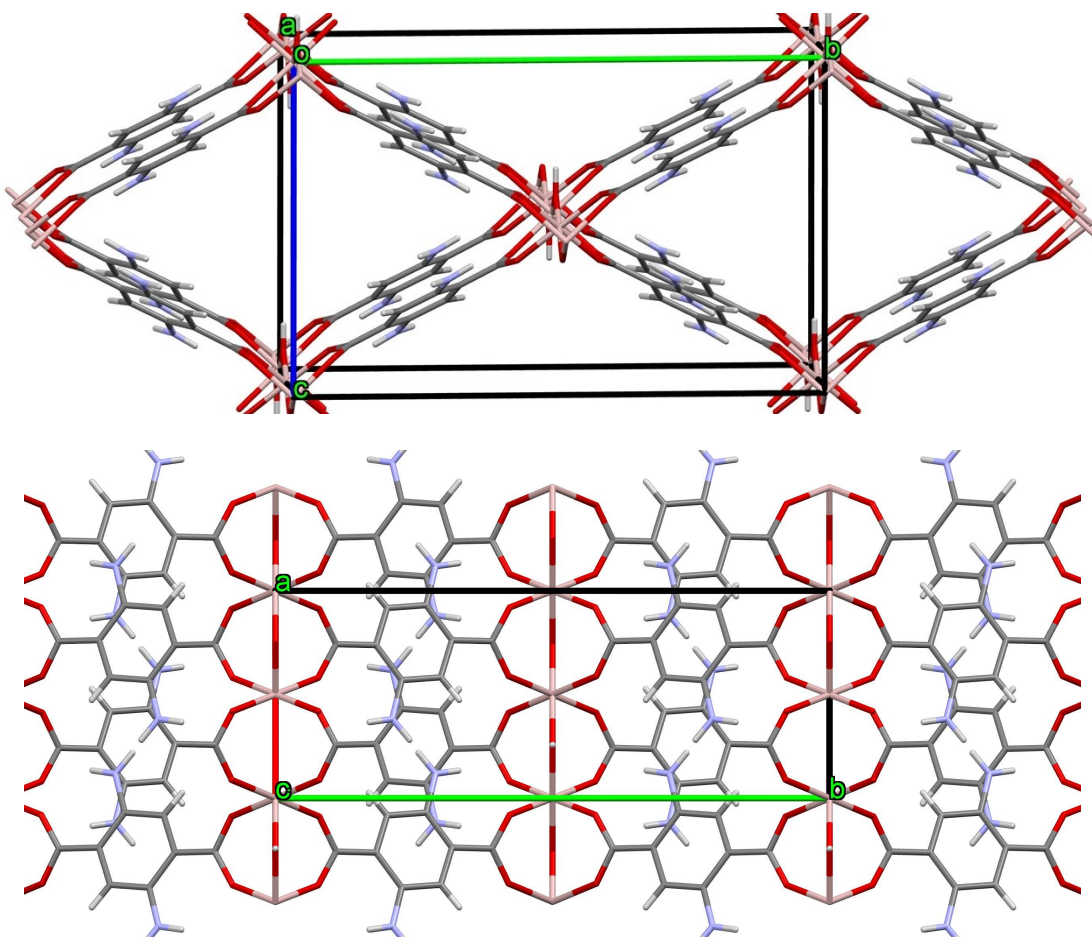**Figure S9**. A portion of the 3D framework (without solvent molecules in pores) in the monoclinic *I2/m* crystal structure of NH₂-MIL-53(Al) viewed in two opposite directions: approximately along axis *a* (top) and along axis *c* (bottom).
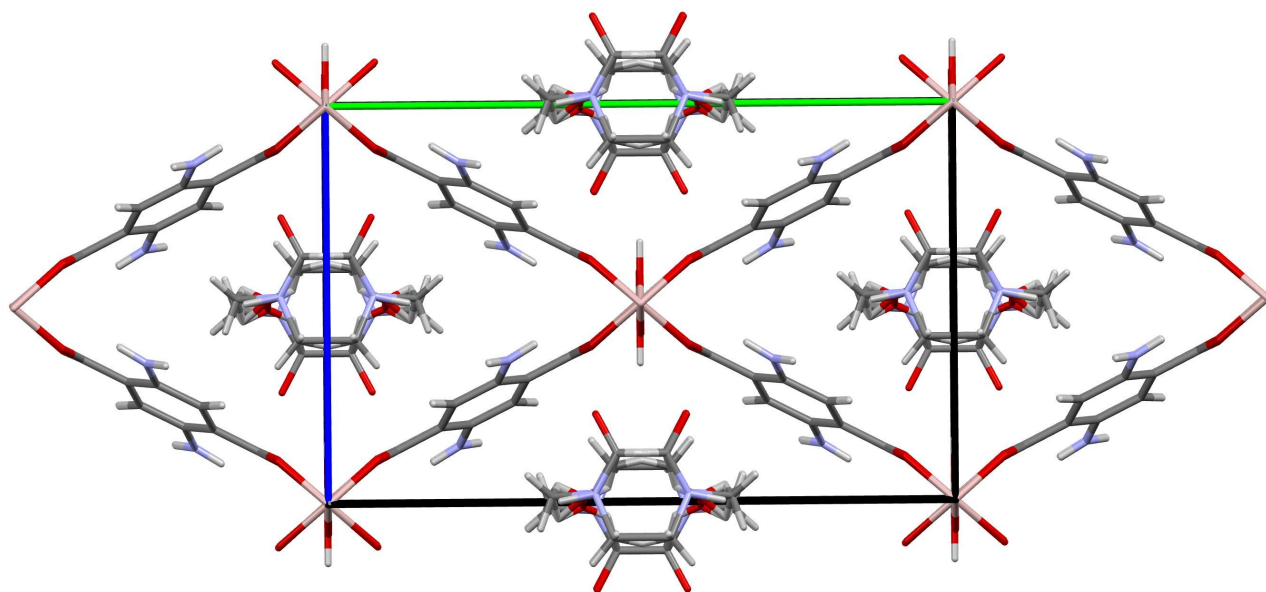

Figure S10. A portion of the monoclinic *I2/m* crystal structure of NH2-MIL-53(Al) with disordered solvent molecules into pores viewed along axis *a*.

References.

[1]. Couck *et al.* (Serra-Crespo) 2012, *ChemSusChem*, **5**, 740

[2]. Werner, P.-E., Eriksson, L., Westdahl, M. (1985) *J.Appl. Cryst.* **18**, 367−370.

[3]. Boultif, A., Louer, D. (2004). *J. Appl. Cryst.* **37**, 724−731.

[4]. Zlokazov, V. B. (1992). *J. Appl. Cryst.* **25**, 69−72.

[5]. Zlokazov, V. B. (1995). *Comput. Phys. Commun.* **85**, 415−422.

[6]. Pawley, G. S. (1981). *J. Appl. Cryst.* **14**, 357−361.

[7]. Zhukov, S. G., Chernyshev, V. V., Babaev, E. V., Sonneveld, E. J., Schenk, H. (2001) *Z.Kristallogr.* **216**, 5−9.

[8]. Chernyshev, V. V., Schenk, H. (1998). *Z. Kristallogr.* **213**, 1−3.

[9]. Isaeva, V.I. Belyaeva, E.V. Fitch, A.N. Chernyshev, V.V., Klyamkin, S.N. Kustov, L.M. (2013). *Cryst. Growth Des.* **13**, 5305-5315.

[10]. Chernyshev, V.V., Morozov, Yu. N., Bushmarinov, I. S., Makoed, A. A., Sergeev, G. B. (2016). *Crystal Growth & Design*, **16**, 1088-1095.

[11]. Veselovsky, V.V., Lozanova, A.V., Isaeva, V.I., Lobova, A.A., Fitch, A.N., Chernyshev, V.V. (2018). *Acta Cryst.* **C74**, 248-255.

[12]. Zlokazov, V. B., Chernyshev, V. V. (1992). *J. Appl. Cryst.* **25**, 447−451.

[13]. Popa, N. C. (1998). *J. Appl. Cryst.* **31**, 176–180.

[14]. Macrae, C. F., Bruno, I. J., Chisholm, J. A., Edgington, P. R., McCabe, P., Pidcock, E., Rodriguez-Monge, L., Taylor, R., van de Streek, J. & Wood, P. A. (2008). *J. Appl. Cryst.* **41**, 466–470.

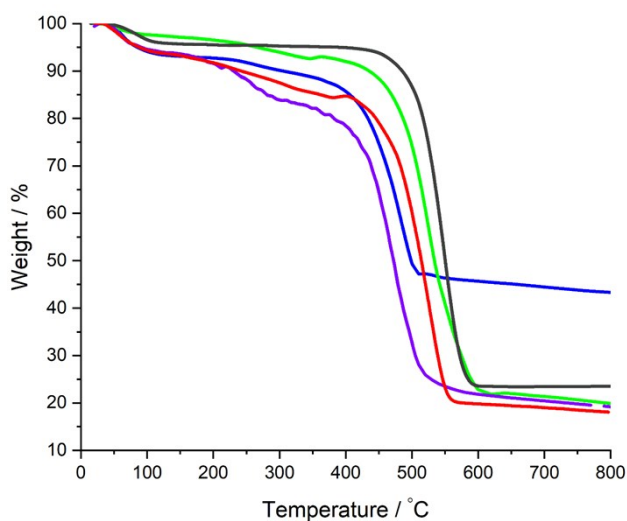**V.** *Study of the thermal stability of MIL-53(Al) type materials*

Figure S11. Temperature dependence of the mass loss (TG-curves) for MIL-53(Al) (dark grey), **MixL3R** (green), **MixL1R** (red), **MixL2R** (blue), NH_2-MIL-53 (violet) during temperature-programmed heating.

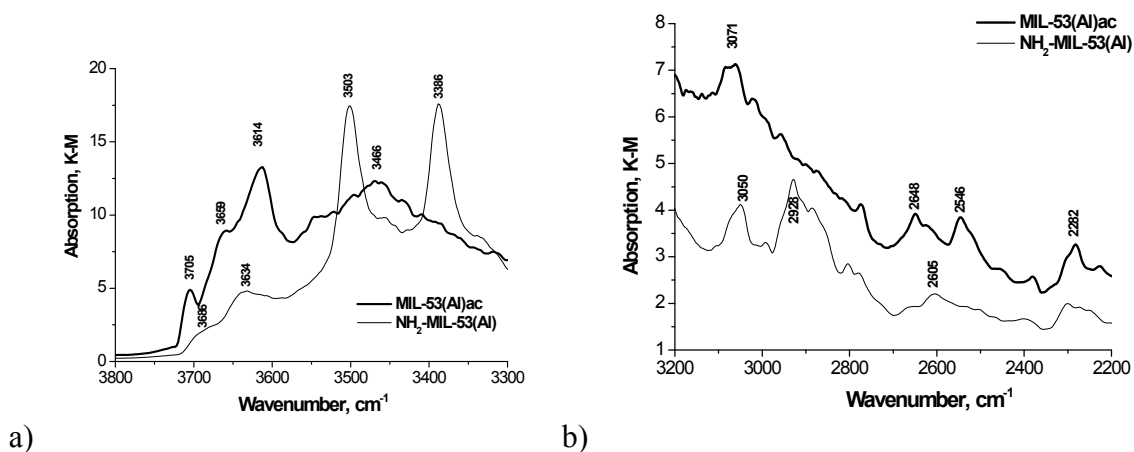**VI**. *DRIFTS investigations of MIL-53(Al) type materials*

a)   b)

Figure S12. The comparison of DRIFT spectra of MIL-53(Al)$_{ac}$ and NH_2-MIL-53(Al) samples in a regions of 3800-3300 cm^{-1} (a) and 3200-2200 cm^{-1} (b).
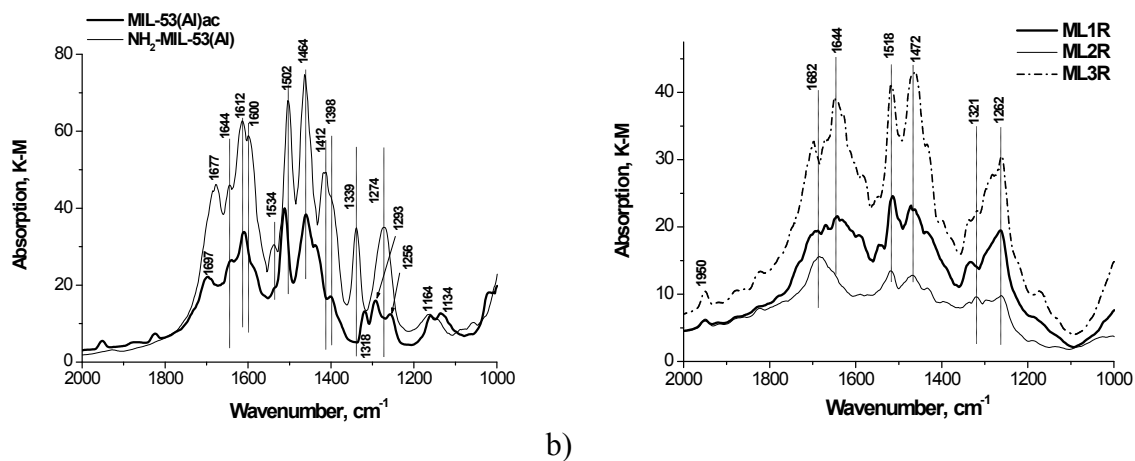
a)   b)

Figure S13. The comparison of DRIFT spectra in 2000-1000 cm^{-1} region of MIL-53(Al)$_{ac}$ and NH$_2$-MIL-53(Al) samples (a), and **MLR** samples (b).

VII. *Study of the pH effect on the 2,4-D adsorption on MixL2R material*
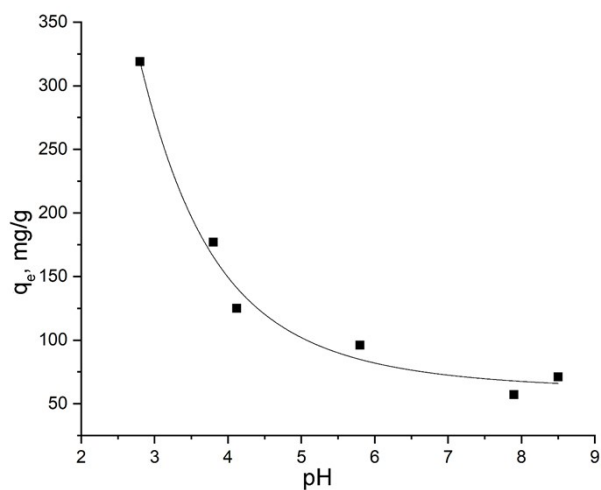

Figure S14. Effect of pH of 2,4-D solution on the adsorbed amount of 2,4-D over **MixL2R** material. 2,4-D concentration: 200 mg/l; adsorption time: 24 h.